www.ijarp.com ISSN 2456-9992 Page: 01-18

International Journal Advanced Research Publications

Research Article

Volume: 02
Issue: 08

COMPUTATIONAL FRAMEWORK FOR ASSESSING WIND-INDUCED INTERFERENCE BETWEEN ADJACENT HIGH-RISE BUILDINGS

Tara Chand Kumawat*, Er. Vinod Kumar Modi

Department of Civil Engineering, Kautilya Institute of Technology and Engineering, Sitapura, Jaipur.

Article Received: 13 July 2026, Article Revised: 02 August 2026, Published on: 22 August 2026

***Corresponding Author: Tara Chand Kumawat**

Department of Civil Engineering, Kautilya Institute of Technology and Engineering, Sitapura, Jaipur.

Doi: https://doi-doi.org/101555/ijarp.4945

ABSTRACT

Aerodynamic interference between neighboring high-rise buildings can redistribute façade pressure and amplify global forces and moments beyond isolated-building estimates. This manuscript establishes a publication-oriented computational fluid dynamics (CFD) framework for assessing two adjacent rectangular prisms while maintaining a strict distinction between supplied evidence and demonstration-only material. The proposed workflow combines a neutral atmospheric boundary-layer inlet, Reynolds-averaged Navier–Stokes screening with the Realizable k–ε closure, domain and mesh-quality controls, empty-domain inflow verification, grid and time-step sensitivity assessment, benchmark validation, and uncertainty-aware post-processing. Interference is quantified using local pressure coefficients and response-specific ratios for along-wind force, across-wind force, and torsional moment. The only supplied numerical result shows that the interfering configuration changes the mean face coefficients from 0.94 to 1.02 on Face A and from −0.78, −0.80, and −0.78 to −0.56, −0.67, and −0.56 on Faces B–D, respectively. These values imply an 8.5% increase in positive pressure on Face A and reductions of 28.2%, 16.3%, and 28.2% in suction magnitude on Faces B–D. Because no solver files, mesh study, benchmark comparison, or time histories were supplied, no validated conclusion is drawn for spacing, height ratio, wind direction, fluctuating response, or torsional amplification. The revised framework identifies the evidence required to convert the demonstration study into a reproducible numerical investigation suitable for peer review.

KEYWORDS: Atmospheric boundary layer; computational fluid dynamics; high-rise buildings; interference factor; pressure coefficient; urban aerodynamics; verification and validation; wind engineering.

1. INTRODUCTION

Urban densification increasingly places tall buildings within one another's aerodynamic influence. A neighboring tower may shield the target building, accelerate flow through a gap, redirect separated shear layers, or expose the target to an unsteady wake. Consequently, façade pressures and integrated loads can differ materially from isolated-building values. The sign of the change is not predetermined: the same arrangement can reduce a mean force while increasing local suction, torsion, or fluctuating response. These distinctions are important for the main wind-force-resisting system, cladding design, serviceability, and occupant comfort [1–12].

Boundary-layer wind-tunnel testing remains the reference approach for complex interference problems. CFD is nevertheless valuable for systematic screening because it offers spatially resolved pressure and flow fields and permits efficient exploration of spacing, height ratio, stagger, and wind direction [13–22]. Its credibility depends on the numerical question being matched to the turbulence model and on transparent verification and validation. Steady RANS may support mean-flow screening, whereas vortex-driven fluctuations, peak loads, and spectra generally require unsteady modeling and statistically converged sampling. Domain extent, atmospheric-boundary-layer consistency, wall treatment, discretization, mesh resolution, and numerical uncertainty must be documented rather than treated as implementation details [14,15,31–35].

1.1 Research gap and novelty

Many interference studies report a maximum amplification without fully disclosing the isolated reference, response definition, sampling basis, or numerical uncertainty. This can obscure whether a reported factor refers to a signed mean, an absolute mean, an RMS quantity, or a peak. A second recurring gap is the use of inlet profiles that are not demonstrably maintained between the inlet and the building location. A third is the interpretation of attractive flow visualizations without establishing grid sensitivity or benchmark agreement. The present contribution is therefore methodological: it integrates response definitions, evidence labeling, a staged verification-and-validation framework, and a reproducible reporting matrix in one manuscript. The contribution is not a claim of a completed parametric CFD campaign; solver-generated results are still required.

1.2 Objectives and research questions

- Quantify how adjacency changes the signed mean pressure coefficient on each principal face.
- Define unambiguous interference factors for local pressure, global forces, and torsional moment.
- Establish a defensible case matrix for spacing, relative height, stagger, and wind incidence.
- Specify mesh, convergence, sampling, validation, and uncertainty evidence required for credible numerical conclusions.
- Relate validated pressure and load changes to gap flow, shielding, wake impingement, asymmetric separation, and vortex interaction.

2. Numerical methodology

2.1 Geometry, coordinates, and configuration parameters

Two rectangular-prism buildings are defined by width B, depth D, and target-building height H_1. The neighboring height is H_2, the minimum clear spacing is s, and wind incidence θ is measured consistently from the positive streamwise reference axis. Building 1 is the target; Building 2 is the interfering neighbor. The source manuscript proposes $s/B = 0.5–5.0$, $H_2/H_1 = 0.75–1.25$, and $\theta = 0°–180°$ as a demonstration envelope. Exact B, D, H_1, stagger offset, model scale, and façade labels remain project-specific inputs.

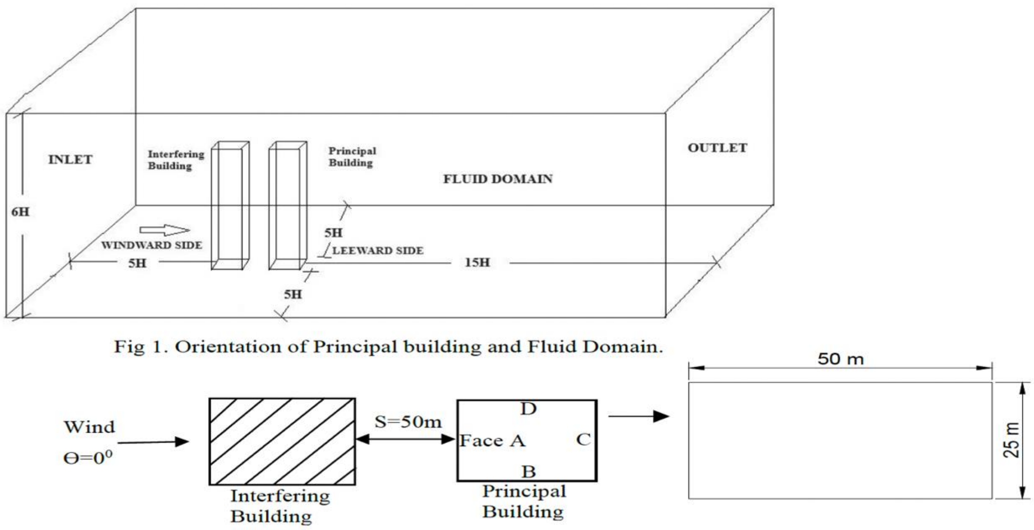

Figure 1. Conceptual two-building geometry and parametric variables. This is a schematic definition, not a solver-domain image; replace dimensions and orientation with the final CAD configuration.

Figure 1 establishes the geometric variables that control interference: normalized spacing, relative height, and wind incidence. Keeping the target and neighboring buildings explicitly identified is essential because shielding and wake exposure are not reciprocal when heights or positions differ. The schematic also shows why the final manuscript must define whether s denotes clear or center-to-center spacing and must preserve one wind-angle convention in the geometry, case matrix, and post-processing. Because no project dimensions are encoded in this diagram, it supports case definition only and cannot be used to infer aerodynamic behavior.

2.2 Governing equations and turbulence closure

For a neutrally stratified, incompressible flow, the Reynolds-averaged conservation equations are written as

$\partial U_i/\partial x_i = 0$(1)

$\rho(\partial U_i/\partial t + U_j\partial U_i/\partial x_j) = -\partial P/\partial x_i + \partial[2\mu S_{ij} - \rho u_i' u_j']/\partial x_j$(2)

$S_{ij} = ½(\partial U_i/\partial x_j + \partial U_j/\partial x_i)$(3)

The Reynolds stresses are closed with the Realizable k–ε eddy-viscosity model [23]. This closure is retained from the source manuscript as a computationally efficient option for screening mean pressures and mean loads. It should not be presented as sufficient evidence for peak, RMS, spectral, or vortex-lock-in quantities unless an unsteady formulation, adequate temporal resolution, and statistical convergence are demonstrated. A model-sensitivity comparison against SST k–ω and, where fluctuating response is central, an appropriate scale-resolving method is recommended.

2.3 Computational domain and boundary conditions

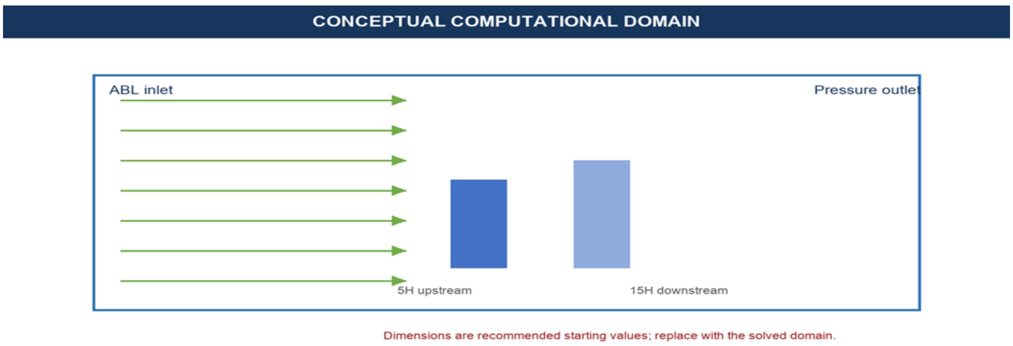

Figure 2. Conceptual computational-domain layout. Dimensions are recommended starting values and must be replaced by the actual solved domain.

Figure 2 translates the physical problem into a boundary-condition framework. The long downstream region is intended to accommodate wake recovery, while the upstream, lateral, and top clearances reduce artificial acceleration and boundary interaction. The inlet arrows represent an atmospheric boundary layer rather than a uniform approach flow. These proportions are starting recommendations; credibility requires reporting the actual H-normalized dimensions, blockage ratio, and a domain-sensitivity or guideline-based justification for the solved model.

Table 1. Boundary-condition reporting requirements for an atmospheric-boundary-layer CFD model.

Boundary	Recommended treatment	Evidence to report
Inlet	Neutral ABL profiles U(z), k(z), and ε(z)	Equations, z_0 or power exponent, u*, reference speed/height, turbulence intensity
Outlet	Pressure outlet; sufficient downstream recovery	Backflow treatment and pressure reference
Top/lateral	Symmetry or slip, sufficiently remote	Distances from buildings and blockage ratio
Ground	No-slip rough wall consistent with inlet ABL	Equivalent sand-grain roughness and roughness constant
Buildings	No-slip wall	Wall treatment and y^+ distribution

Domain dimensions should be expressed in H_1 and justified against recognized wind-engineering guidance [14,15]. A useful starting point is at least $5H_1$ upstream, $15H_1$ downstream, $5H_1$ to each lateral boundary, and $5H_1$ above the roof, followed by a blockage and sensitivity check. These values are recommendations—not supplied project settings. Before buildings are introduced, an empty-domain simulation should confirm that the inlet velocity and turbulence profiles remain acceptably homogeneous at the intended building plane.

$$U(z) = (u^*/\kappa) \ln[(z + z_0)/z_0] \quad (4)$$

$$k(z) = u^{*2}/\sqrt{C\mu} \quad (5)$$

$$\varepsilon(z) = u^{*3}/[\kappa(z + z_0)] \quad (6)$$

Equations (4)–(6) show a common equilibrium logarithmic inlet. The adopted expressions must be compatible with the ground-wall roughness implementation and the selected solver.

If a power law is used instead, its exponent, reference quantities, and terrain justification must be stated.

2.4 Spatial and temporal discretization

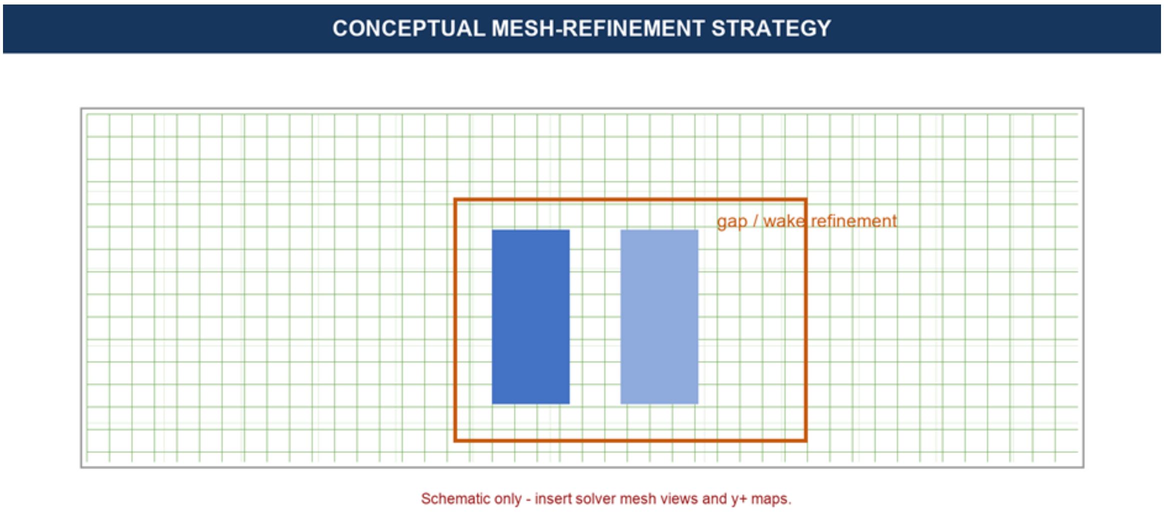

Figure 3. Conceptual mesh-refinement strategy. Replace with solver-exported mesh sections, inflation-layer detail, quality metrics, and wall y^+ maps.

Figure 3 identifies the regions where discretization error is most likely to affect the predicted interference: building corners, the inter-building gap, separated shear layers, and the near wake. Local refinement in these regions should be accompanied by gradual transitions to the background grid and near-wall layers consistent with the selected wall treatment. The diagram is not evidence of mesh adequacy. The submitted study should replace it or supplement it with solver mesh sections, cell-quality statistics, a wall-y+ distribution, and systematic grid-sensitivity results.

Use second-order spatial schemes for momentum and turbulence variables after a stable initialization. Refine the mesh at building edges, in the gap, along separated shear layers, near roof corners, and through the near wake. Inflation layers should be designed for the selected wall treatment. Report cell count, minimum and maximum cell size normalized by B, layer count and growth rate, quality statistics, y^+ distribution, pressure–velocity coupling, gradient reconstruction, solver precision, under-relaxation or time-marching settings, and software/version.

For transient calculations, select the time step using both a convective criterion and a time-step sensitivity test. Report the maximum Courant number in critical regions, startup duration discarded, sampling duration, sampling frequency, number of shedding cycles, and statistical stationarity. Mean and RMS histories should be monitored in addition to algebraic residuals.

2.5 Verification, validation, and uncertainty framework

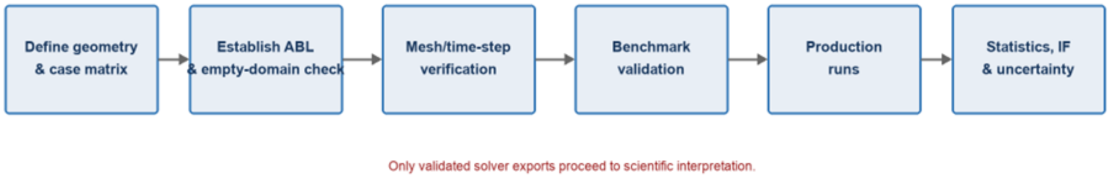

Figure 4. Proposed evidence-gated numerical workflow. The diagram describes the required process and does not report completed simulations.

Figure 4 emphasizes that production cases should be interpreted only after a sequence of numerical credibility checks. Geometry and inflow definition precede empty-domain ABL verification; mesh/time-step studies establish numerical sensitivity; and benchmark validation assesses model-form performance before the parametric campaign is evaluated. This ordering reduces the risk of attributing numerical artifacts to building interference. The final statistics and uncertainty stage must also preserve traceability from each plotted value to a case file and processing method.

Table 2. Verification, validation, and uncertainty evidence required before interpreting the parametric cases.

Stage	Minimum comparison	Acceptance/reporting output
Iterative convergence	Residuals plus forces/moments and face-averaged C_p	Stable monitored quantities; stated residual criteria
Grid sensitivity	Coarse, medium, fine systematically refined meshes	Changes in key coefficients; refinement ratio; GCI when asymptotic behavior is supported [34]
Time-step sensitivity	At least two, preferably three, time steps for URANS/hybrid runs	Mean, RMS, peak, dominant frequency, and Courant statistics
ABL verification	Empty-domain target vs. incident profiles at building plane	Profile plots and quantitative deviation over $0 < z \leq H_1$

Stage	Minimum comparison	Acceptance/reporting output
Validation	Isolated-building benchmark with matching geometry/ABL	C_p distributions and integrated coefficients with MAE, NRMSE, bias, correlation
Model sensitivity	Realizable k–ε vs. alternative closure	Model-form effect on critical quantities

$GCI_{21} = F_s\,|(\varphi_1 - \varphi_2)/\varphi_1|\,/(r^p - 1)$(7)

Here φ_1 and φ_2 are fine- and medium-grid solutions, r is the representative refinement ratio, p is the observed order, and F_s is a safety factor [34]. GCI should be reported only when the grid family and solution behavior support its assumptions. Otherwise, report transparent percentage changes and discuss non-monotonicity.

2.6 Case matrix

Table 5. Source-manuscript demonstration case matrix. None of these cases is confirmed by supplied solver input or output files.

Case	s/B	H_2/H_1	θ (°)	Status / purpose
S05	0.5	1.00	0	Demonstration case; close gap
S10	1.0	1.00	0	Demonstration case; proposed critical spacing
S15	1.5	1.00	0	Demonstration case; intermediate
S20	2.0	1.00	0	Demonstration case; intermediate
S30	3.0	1.00	0	Demonstration case; weak interference
S40	4.0	1.00	0	Demonstration case; near-isolated
S50	5.0	1.00	0	Demonstration reference
H075	1.0	0.75	0	Demonstration case; lower neighbor
H125	1.0	1.25	0	Demonstration case; taller neighbor
A-SWEEP	1.0	1.00	0–180	Demonstration directional sweep; increment unspecified

2.7 Quantities of interest and normalization

$C_p(x,t) = [p(x,t) - p_\infty]/q_{ref}, \quad q_{ref} = \tfrac{1}{2}\rho U_{ref}^2$(8)

$C\_F = F/(q_{ref} A_{ref}), \quad C\_M = M/(q_{ref} A_{ref} L_{ref})$(9)

$IF\_Q = Q_{int}/Q_{iso}$(10)

$IF\_|Cp| = |C_{p,int}|/|C_{p,iso}|$ (suction magnitude only)(11)

The isolated and interfering quantities must use identical reference speed, area, length, coordinate system, averaging window, and statistical definition. Signed ratios should be avoided when the denominator approaches zero. For each result, identify whether Q is a mean, RMS, peak, percentile, or spectral ordinate. Report confidence intervals or block-to-block variability for transient statistics.

3. RESULTS

3.1 Supplied face-pressure coefficients

The supplied mean face coefficients are reproduced without alteration in Table 6. Face A changes from 0.94 in the isolated configuration to 1.02 with interference, corresponding to ΔC_p = +0.08 and an 8.5% increase in positive pressure. On Faces B, C, and D, the coefficients become less negative. Their suction magnitudes decrease by 28.2%, 16.3%, and 28.2%, respectively. These are face-level values; they do not establish local peak cladding pressure or a global load without the underlying spatial integration and normalization.

Table 6. Supplied surface-pressure coefficients and derived signed/magnitude comparisons. The provenance, averaging interval, face-averaging method, configuration, and uncertainty were not supplied.

Face	$C_{p,int}$	$C_{p,iso}$	ΔC_p	$\lvert C_{p,int}\rvert/\lvert C_{p,iso}\rvert$	Magnitude change
A	1.02	0.94	+0.08	1.085	+8.5%
B	−0.56	−0.78	+0.22	0.718	−28.2%
C	−0.67	−0.80	+0.13	0.838	−16.3%
D	−0.56	−0.78	+0.22	0.718	−28.2%

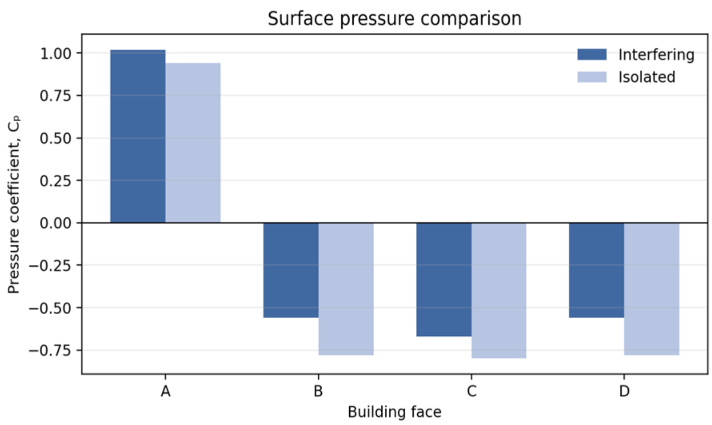

Figure 5. Comparison of the supplied face-pressure coefficients. The chart reproduces the values in Table 6; it is not a validation comparison.

Figure 5 is the only result figure based on supplied numerical values. It shows that the interfering case raises the positive coefficient on Face A from 0.94 to 1.02, while the negative coefficients on Faces B-D move toward zero. Thus, adjacency produces pressure redistribution rather than uniform amplification: windward loading increases, whereas the supplied suction magnitudes decrease. The plot does not reveal local peaks, vertical variation, statistical uncertainty, or the resulting integrated force and torsion, so those quantities cannot be inferred from this face-level comparison alone.

3.2 Spacing sensitivity—required solver output

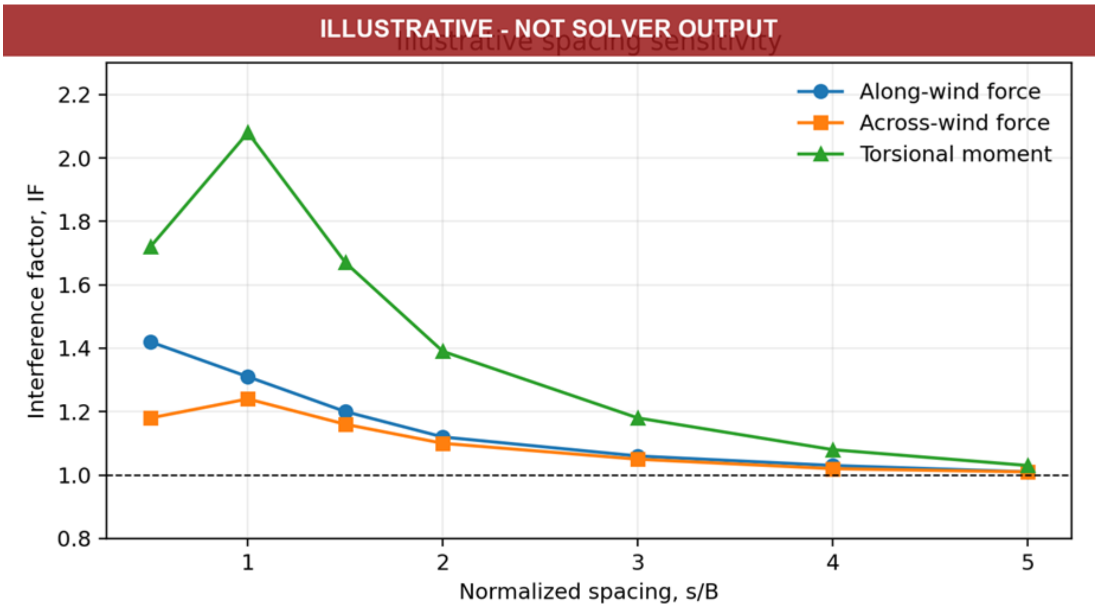

Figure 6. Illustrative spacing-sensitivity chart reproduced from the source and watermarked. Values are synthetic demonstration data, not CFD results.

Figure 6 illustrates the presentation expected for a spacing study: interference factors are compared against the isolated reference IF = 1 as s/B increases. Within the synthetic series, all three responses tend toward unity with separation, and the illustrative torsional curve is more sensitive than the force curves at close spacing. This pattern is physically plausible because gap confinement and asymmetric wake interaction generally weaken with distance, but it is not a CFD finding. The curves and Table 7 must be replaced with solver exports, uncertainty estimates, and the exact configuration before any critical spacing or decay distance is reported.

Table 7. Synthetic spacing-series values represented in Figure 6. Replace every value with a traceable solver export.

s/B	IF along-wind	IF across-wind	IF torsion	Evidence status
0.5	1.42	1.18	1.72	Synthetic
1.0	1.31	1.24	2.08	Synthetic
1.5	1.20	1.16	1.67	Synthetic
2.0	1.12	1.10	1.39	Synthetic
3.0	1.06	1.05	1.18	Synthetic
4.0	1.03	1.02	1.08	Synthetic
5.0	1.01	1.00	1.02	Synthetic

3.3 Relative-height sensitivity—required solver output

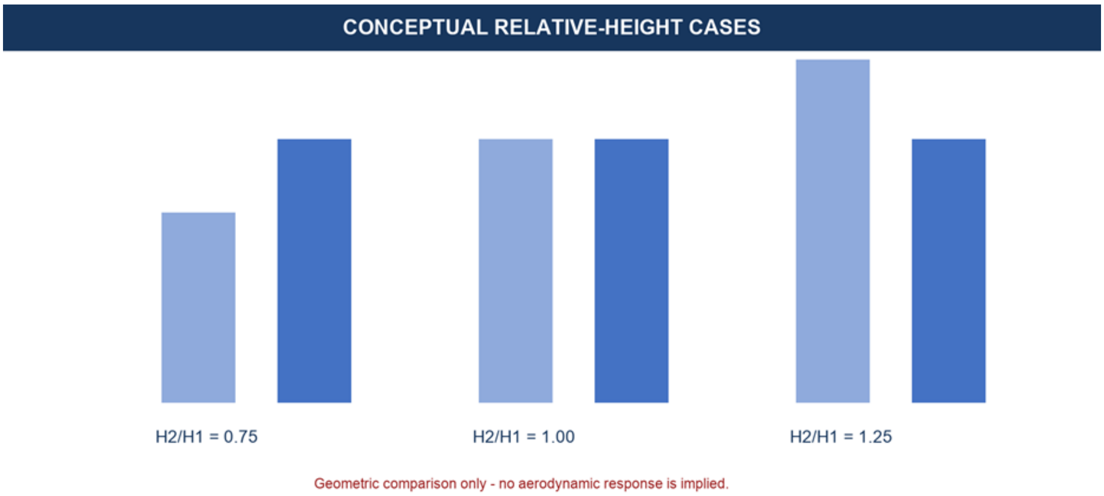

Figure 7. Conceptual relative-height configurations. The diagram contains no aerodynamic result.

Figure 7 isolates the geometric role of relative height. A lower neighbor may shelter only the lower portion of the target, an equal-height neighbor may influence most of its elevation, and a taller neighbor may expose the target to a vertically varying wake. These statements describe possible exposure regimes, not predicted responses. Solver-derived pressure profiles and integrated coefficients are required to determine whether each configuration shields or amplifies loading and whether the governing effect occurs near the base, mid-height, or roof.

3.4 Directional sensitivity—required solver output

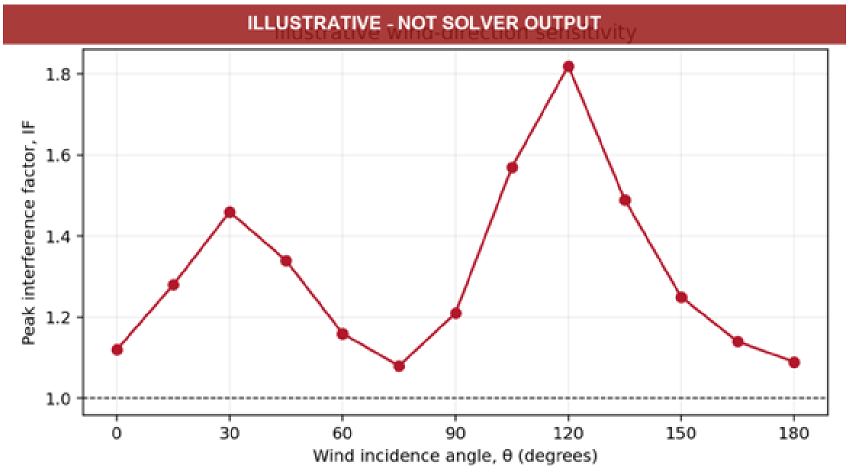

Figure 8. Illustrative directional-sensitivity chart reproduced from the source and watermarked. The reported maximum is synthetic.

Figure 8 demonstrates why interference should be evaluated over a directional envelope. In the synthetic curve, the response varies non-monotonically and its illustrative maximum occurs at an oblique angle rather than at 0° or 90°. Such behavior can arise as projected blockage, gap alignment, separation points, and wake impingement change with wind direction. However, neither the reported peak nor its angle is validated. The final figure should state the angular increment, response statistic, configuration, uncertainty, and whether intermediate angles were refined around the apparent maximum.

Table 9. Synthetic directional-series values represented in Figure 8. Replace with solver-generated directional results and uncertainty.

θ (°)	Peak IF	Status	θ (°)	Peak IF	Status
0	1.12	Synthetic	105	1.57	Synthetic
15	1.28	Synthetic	120	1.82	Synthetic
30	1.46	Synthetic	135	1.49	Synthetic
45	1.34	Synthetic	150	1.25	Synthetic
60	1.16	Synthetic	165	1.14	Synthetic
75	1.08	Synthetic	180	1.09	Synthetic
90	1.21	Synthetic			

3.5 Flow topology and pressure fields—required solver output

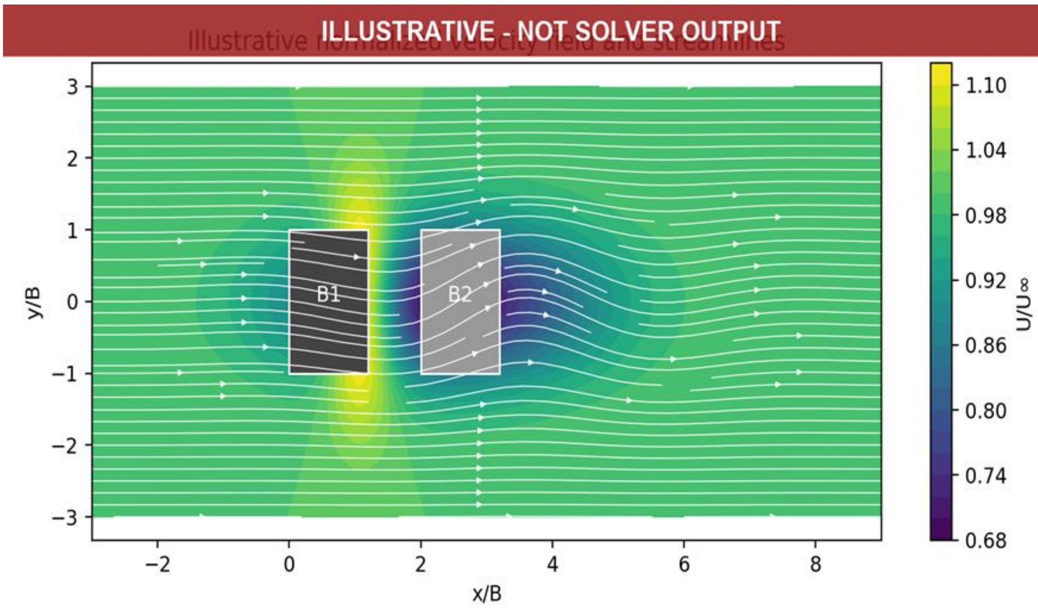

Figure 9. Illustrative normalized velocity field and streamlines reproduced from the source. This is a synthetic visualization, not a CFD solver export.

Figure 9 provides a qualitative visualization of the mechanisms that a solved flow field should be used to test. The illustration suggests acceleration in the gap, flow diversion around the upstream building, and a lower-momentum wake downstream; these features could redistribute surface pressure and create asymmetric loading. Because the field is synthetic, streamline shape and velocity magnitude must not be interpreted quantitatively. A valid comparison should use solver-exported mean and instantaneous fields, identical normalization and color limits, declared planes, and complementary pressure and vorticity information.

Table 10. Required solver-exported flow-field panels and comparability controls.

Required CFD panel	Plane / location	Normalization	Comparison rule	Status
Mean velocity magnitude	Horizontal z/H_1 = [insert]	U/Uref	Same color limits	Awaiting solver output
Mean pressure coefficient	Building surfaces	C_p	Same contour levels	Awaiting solver output
Vorticity or Q-criterion	Declared plane/iso-value	Dimensionless form stated	Matched thresholds	Awaiting solver output
Instantaneous velocity	Declared time/phase	U/Uref	Separate from mean	Awaiting solver output
Wall y^+	All building surfaces	y^+	Report range/distribution	Awaiting solver output

3.6 Demonstration-only source trends

The source manuscript included a synthetic spacing sweep, a synthetic directional sweep, and a synthetic velocity field to demonstrate possible presentation formats. It reported a torsional interference factor of 2.08 at $s/B = 1.0$ and a directional peak of 1.82 at $\theta = 120°$. These values are preserved here only as an audit trail of the supplied document; they must not appear in an abstract, conclusion, design recommendation, or comparison with literature unless reproduced by a verified and validated solver campaign.

4. DISCUSSION

The supplied face coefficients demonstrate that interference is spatially nonuniform. Increased positive pressure on Face A occurs simultaneously with reduced suction magnitude on Faces B–D. This prevents the use of one universal multiplier for every façade or response component. Global drag, lift, and torsion must be calculated by integrating the resolved pressure field with the correct lever arms. A face-average value can conceal local corner peaks that govern cladding, while a small change in net force can coexist with a substantial torsional change if the pressure redistribution is asymmetric.

Several mechanisms could explain such redistribution—shielding, gap acceleration, shear-layer deflection, wake impingement, and altered separation—but the supplied values alone cannot identify which mechanism occurred. Mechanistic interpretation must be tied to validated pressure contours, velocity and vorticity fields, and the exact arrangement. Causal language should be reserved for comparisons that show both the load change and the corresponding flow structure under matched normalization.

The Realizable k–ε model is a pragmatic mean-flow screening tool, but eddy-viscosity RANS closures can suppress or misrepresent unsteady anisotropic wake structures. Therefore, any claim concerning fluctuating lift, peak torsion, vortex shedding, or spectral response should be supported by URANS with convergence evidence or, preferably where resources allow, a validated scale-resolving simulation. Model sensitivity should be incorporated into uncertainty rather than discussed only as a limitation.

4.1 Engineering implications

- Assess critical façade zones and global structural actions separately.
- Use a directional envelope that includes oblique winds; cardinal directions alone may not bound the response.
- Carry the same isolated reference and normalization through every interference comparison.
- Escalate configurations with large mean or asymmetric pressure changes to transient analysis and, for final design, boundary-layer wind-tunnel confirmation where required.
- Do not transfer interference factors between geometrically or aerodynamically dissimilar urban arrangements without evidence.

4.2 LIMITATIONS

The source package did not include project dimensions, CAD geometry, solver setup, boundary-condition files, meshes, convergence histories, sampling records, pressure taps or surface fields, integrated load histories, benchmark data, or uncertainty estimates. The provenance and statistical definition of the four supplied face coefficients are also unknown. Accordingly, this paper is a scientifically structured reporting framework with one small supplied dataset—not a validated parametric CFD study. Its principal limitation must remain explicit until the missing evidence is provided.

5. CONCLUSIONS

1. The supplied face-pressure coefficients show a nonuniform interference effect: Face A increases from $C_p = 0.94$ to 1.02, whereas suction magnitudes on Faces B–D decrease by 28.2%, 16.3%, and 28.2%, respectively.

2. These face-level changes cannot, by themselves, establish global along-wind, across-wind, or torsional amplification; spatial fields, integration definitions, and reference quantities are required.
3. No validated conclusion can presently be drawn for spacing, relative height, wind direction, fluctuating response, or flow mechanism because the corresponding source results are synthetic.
4. A defensible study should complete empty-domain ABL verification, grid and time-step sensitivity, isolated-building benchmark validation, turbulence-model sensitivity, and statistically converged post-processing before interpreting the case matrix.
5. The revised figures and tables provide an auditable pathway for replacing demonstration material with solver-generated evidence without changing the manuscript's scientific structure.

REFERENCES

1. ASCE. ASCE/SEI 7-22: Minimum Design Loads and Associated Criteria for Buildings and Other Structures. Reston, VA: American Society of Civil Engineers; 2022.
2. Bureau of Indian Standards. IS 875 (Part 3):2015: Design Loads (Other Than Earthquake) for Buildings and Structures—Code of Practice, Part 3 Wind Loads. New Delhi: BIS; 2015.
3. CEN. EN 1991-1-4: Eurocode 1: Actions on Structures—Part 1-4: General Actions—Wind Actions. Brussels: European Committee for Standardization; 2005.
4. Architectural Institute of Japan. Recommendations for Loads on Buildings. Tokyo: AIJ; 2015.
5. Davenport AG. The application of statistical concepts to the wind loading of structures. Proc Inst Civ Eng. 1961;19:449–472.
6. Melbourne WH. Wind environment studies in Australia. J Wind Eng Ind Aerodyn. 1978;3:201–214.
7. Taranath BS. Wind and Earthquake Resistant Buildings: Structural Analysis and Design. New York: Marcel Dekker; 2005.
8. Kareem A. Wind-induced response analysis of tension leg platforms. J Struct Eng. 1985;111:37–55.
9. Kawai H. Pressure fluctuations on square prisms—some practical problems. J Wind Eng Ind Aerodyn. 1982;10:97–110.

10. Kwok KCS, Melbourne WH. Wind-induced lock-in excitation of tall structures. J Wind Eng Ind Aerodyn. 1981;8:135–149.
11. Vickery BJ. Fluctuating lift and drag on a long cylinder of square cross-section in a smooth and in a turbulent stream. J Fluid Mech. 1966;25:481–494.
12. Tamura T. Towards practical use of LES in wind engineering. J Wind Eng Ind Aerodyn. 2008;96:1451–1478.
13. Blocken B. Computational fluid dynamics for urban physics: importance of the form of the governing equations, turbulence models and numerical methods. Build Environ. 2015;91:219–245.
14. Tominaga Y, Mochida A, Yoshie R, et al. AIJ guidelines for practical applications of CFD to pedestrian wind environment around buildings. J Wind Eng Ind Aerodyn. 2008;96:1749–1761.
15. Franke J, Hirsch C, Jensen AG, et al. Recommendations on the Use of CFD in Wind Engineering. COST Action C14. Brussels; 2004.
16. Britter RE, Hanna SR. Flow and dispersion in urban areas. Annu Rev Fluid Mech. 2003;35:469–496.
17. Fernando HJS. Fluid dynamics of urban atmospheres in complex terrain. Annu Rev Fluid Mech. 2010;42:365–389.
18. Oke TR. Street design and urban canopy layer climate. Energy Build. 1988;11:103–113.
19. Mochida A, Lun IYF. Prediction of wind environment and thermal comfort at pedestrian level in urban area. J Wind Eng Ind Aerodyn. 2008;96:1498–1527.
20. Murakami S. Comparison of various turbulence models applied to a bluff body. J Wind Eng Ind Aerodyn. 1993;46–47:21–36.
21. Rodi W. Turbulence Models and Their Application in Hydraulics. Delft: IAHR; 1984.
22. Launder BE, Spalding DB. The numerical computation of turbulent flows. Comput Methods Appl Mech Eng. 1974;3:269–289.
23. Shih TH, Liou WW, Shabbir A, Yang Z, Zhu J. A new k–ε eddy-viscosity model for high Reynolds number turbulent flows. Comput Fluids. 1995;24:227–238.
24. Versteeg HK, Malalasekera W. An Introduction to Computational Fluid Dynamics: The Finite Volume Method. 2nd ed. Harlow: Pearson; 2007.
25. Ferziger JH, Perić M, Street RL. Computational Methods for Fluid Dynamics. 4th ed. Cham: Springer; 2020.
26. Menter FR. Two-equation eddy-viscosity turbulence models for engineering applications. AIAA J. 1994;32:1598–1605.

27. Spalart PR, Allmaras SR. A one-equation turbulence model for aerodynamic flows. AIAA Paper 92-0439; 1992.
28. Pope SB. Turbulent Flows. Cambridge: Cambridge University Press; 2000.
29. Wilcox DC. Turbulence Modeling for CFD. 3rd ed. La Cañada, CA: DCW Industries; 2006.
30. Gatski TB, Speziale CG. On explicit algebraic stress models for complex turbulent flows. J Fluid Mech. 1993;254:59–78.
31. Casey M, Wintergerste T, editors. ERCOFTAC Best Practice Guidelines: Industrial Computational Fluid Dynamics of Single-Phase Flows. Brussels: ERCOFTAC; 2000.
32. Roache PJ. Verification and Validation in Computational Science and Engineering. Albuquerque, NM: Hermosa; 1998.
33. Oberkampf WL, Trucano TG. Verification and validation in computational fluid dynamics. Prog Aerosp Sci. 2002;38:209–272.
34. Celik IB, Ghia U, Roache PJ, Freitas CJ, Coleman H, Raad PE. Procedure for estimation and reporting of uncertainty due to discretization in CFD applications. J Fluids Eng. 2008;130:078001.
35. ASME. V&V 20-2009: Standard for Verification and Validation in Computational Fluid Dynamics and Heat Transfer. New York: ASME; 2009.